Orsay δ protein is required for non-lytic viral egress

Wang Yuan[1*], Ying Zhou[1*], Yanlin Fan[1], Yizhi J. Tao[1#], Weiwei Zhong[1#]

Running title: non-lytic egress of the Orsay virus

[1] Department of BioSciences, Rice University, Houston, Texas, USA

[#] Address correspondence to Yizhi J. Tao ytao@rice.edu, and Weiwei Zhong weiwei.zhong@rice.edu

* These authors contributed equally to this study.

Abstract

Non-enveloped gastrointestinal viruses such as human rotavirus can exit infected cells from the apical surface without cell lysis. The mechanism of such non-lytic exit is poorly understood. The non-enveloped Orsay virus is an RNA virus infecting the intestine cells of the nematode *Caenorhabditis elegans*. Dye staining results suggested that Orsay exits from the intestine of infected worms in a non-lytic manner. Therefore, the Orsay-*C. elegans* system provides an excellent *in vivo* model to study viral exit. The Orsay genome encodes three proteins: RNA-dependent RNA polymerase, capsid protein (CP), and a nonstructural protein δ. δ can also be expressed as a structural CP-δ fusion. We generated an ATG-to-CTG mutant virus that had normal CP-δ fusion but could not produce free δ due to lack of the start codon. This mutant virus showed a viral exit defect without obvious phenotypes in other steps of viral infection, suggesting that δ is involved in viral exit. Ectopically expressed free δ localized near the apical membrane of intestine cells in *C. elegans* and co-localized with ACT-5, an intestine-specific actin that is a component of the terminal web. Orsay infection rearranged ACT-5 apical localization. Reduction of ACT-5 level via RNAi significantly exacerbated the viral exit defect of the δ mutant virus, suggesting that δ and ACT-5 functionally interact to promote Orsay exit. Together, these data support a model that the viral δ protein interacts with the actin network at the apical side of host intestine cells to mediate polarized, non-lytic egress of the Orsay virus.

Importance

An important step of the viral life cycle is how viruses exit from host cells to spread to other cells. Certain non-enveloped viruses can exit cultured cells in non-lytic ways, however, such non-lytic exit has not been demonstrated *in vivo*. In addition, it is not clear how such non-lytic exit is achieved mechanistically *in vivo*. Orsay is a non-enveloped RNA virus that infects the intestine cells of the nematode *C. elegans*. It is currently the only virus known to naturally infect *C. elegans*. Using this *in vivo* model, we show that the δ protein encoded by Orsay facilitates the non-lytic exit of the virus, possibly by interacting with host actin on the apical side of the worm intestine cells.

Introduction

Viral egress is an important step of the viral life cycle. Two mechanisms are commonly employed by viruses to exit host cells, cell lysis and viral exocytosis (1). In cell lysis, viruses are released after the burst of host cells. In viral exocytosis, viruses bud through host cell membranes to reach extracellular space. It is commonly believed that enveloped viruses egress via viral exocytosis and acquire their envelopes when traversing host cell membranes, and that non-enveloped viruses rely on cell lysis to egress. However, several reports demonstrated that non-enveloped viruses could also exit cells via non-lytic pathways. Non-enveloped viruses such as human hepatitis A virus (HAV) (2), poliovirus (3), simian virus 40 (SV40) (4), and rotavirus (5) can all exit polarized cells from the apical surface without cell lysis. The mechanism of this process is poorly understood.

One challenge in studying viral egress is that this process is affected by the host cell physiology. For example, it was reported that the non-lytic egress process of poliovirus may only be observed in polarized cells mimicking natural host cells, and that lysis is required for the same virus to be released from non-polarized cultured cells (3). Therefore, *in vivo* models of viral egress are important to study this host-virus interaction process under natural host cell physiology.

The nematode *Caenorhabditis elegans* has been a successful *in vivo* model for studies of host-pathogen interactions including bacterial pathogens such as *Pseudomonas*, intracellular parasites such as *Nematocida parisii* (6), and lately the intestinal virus Orsay (7). Discovered in 2011, the non-enveloped Orsay virus is currently the only known virus that naturally infects the nematode *C. elegans* (7). Orsay infects *C. elegans* intestine cells

66 and is transmitted horizontally (7). Orsay infection does not affect animal lifespan or
67 brood size, but dramatically changes the morphology of intestine cells: the storage
68 granules disappear; the cytoplasm loses viscosity and becomes fluid; and intermediate
69 filaments become disorganized near the apical border (7). The *C. elegans* intestine
70 consists of 20 large epithelial cells that resemble human intestinal epithelial cells, in that
71 they are both polarized and both have structures such as microvilli and terminal web (8).
72 The *C. elegans* intestine cells can be easily observed *in vivo* because of the transparent
73 body of the worms. Therefore, the *C. elegans*-Orsay system provides an excellent model
74 to study natural host-virus interactions in a live, intact animal.

75 Together with two other nematode viruses, Santeuil and Le Blanc, both of which
76 infect *C. briggsae* (7, 9), Orsay represents a new class of viruses. These three viruses
77 have a bipartite, positive-stranded RNA genome that is distantly related to nodaviruses
78 (7, 9). Their genomes range from 6.3 to 6.5 kb in size with only three open reading
79 frames (ORFs). The RNA1 segment contains one ORF encoding the RNA-dependent
80 RNA polymerase (RdRP); the RNA2 segment contains two ORFs encoding the capsid
81 protein (CP) and δ (7, 9). δ is particularly intriguing as it shows no homology to any
82 sequence in Genbank (7). δ can also be expressed as a CP-δ fusion protein through
83 ribosomal frameshifting (10). CP-δ has been detected in purified viruses, but the
84 expression of free δ has yet to be confirmed (10). It was reported that δ has no RNAi
85 suppression activity (11), unlike nonstructural proteins from related nodaviruses.

86 We have recently shown that δ forms a pentameric filament, and that CP-δ is
87 incorporated into Orsay capsid with an essential role in viral entry (12). Here we show
88 that Orsay exits the host intestine cells in a non-lytic fashion, and that δ is required for

efficient viral egress. δ accumulates near the apical surface of intestine cells, and genetically interacts with host actin. Our data suggest that Orsay uses δ to rearrange host actin at the terminal web to facilitate non-lytic viral exit. These results bring insights into the mechanisms of how non-enveloped viruses achieve polarized non-lytic exit *in vivo*.

Results

Non-lytic egress of Orsay

Several empirical observations suggested that the Orsay virus may utilize a non-lytic exit from the *C. elegans* intestine cells. For example, we have never observed any infected animal with a gap of missing intestine cells that might indicate a lytic exit. The infective animals are alive, and have a similar lifespan as those uninfected worms (7), suggesting that a lytic exit is unlikely for Orsay, considering that the entire *C. elegans* intestine is composed of only 20 large epithelial cells (8). However, it is still possible that the infected intestine cells have damaged cellular integrity while appearing intact at the gross morphology level.

To investigate whether Orsay infection caused damage to the cellular integrity of intestine cells, we fed the animals with propidium iodite (PI), a dye that cannot diffuse through intact cell membrane (13). In normal worms with intact intestine cells, PI stayed in the intestine lumen, and there was no intracellular PI staining (Fig. 1A). As a positive control, worms fed with the *Bacillus thuringiensis* pore-forming toxin Cry5B (14) had extensive intracellular PI staining (Fig. 1B). Orsay-infected animals often had an enlarged intestine lumen possibly caused by constipation, yet the PI staining was limited

111 to the lumen and not in the cytosol (Fig. 1C). Therefore, Orsay infection did not appear to
112 cause any damage to host cell integrity.
113 We quantified the PI staining results on intestine cells. 100% (56/56) of
114 uninfected animals had no intracellular PI staining; 100% (65/65) of Cry5B-treated
115 animals showed intracellular PI staining; 97% (60/62) of Orsay-infected animals showed
116 no intracellular PI staining, while the remaining 3% (2/62) worms were inconclusive due
117 to an over-enlarged and distorted intestine lumen. These data strongly suggested that
118 Orsay exits host cells non-lytically.

119 **δ ATG mutant virus has viral exit defects**

120 To investigate free δ function, we used a reverse genetics system (15) (Fig. 2A) to
121 generate a mutant virus which had an ATG-to-CTG mutation in the start codon of the δ
122 ORF and thus in theory could not produce free δ due to lack of the start codon. Upon
123 infection of the ATG mutant virus, worms showed normal viral load as determined by
124 qRT-PCR (Fig. 2B) and displayed normal viral infection symptoms (12), suggesting that
125 free δ is not required for viral entry or replication. In contrast, the culture medium
126 showed a significantly reduced viral load (Fig. 2B), suggesting a viral exit defect.
127 Considering that the ATG mutation also introduced a M→L amino acid change in
128 CP-δ, we examined the effects of the ATG mutation on viral entry using a worm strain
129 with the transcriptional reporter *F26F2.1p*::*GFP*. This strain expresses GFP upon Orsay
130 exposure presumably due to certain innate immune response (16). Both the ATG mutant
131 virus and the wild-type virus showed similar infection kinetics, with similar percentages
132 of GFP-positive worms at each time point after viral exposure (Fig. 2C), suggesting that
133 the ATG mutant virus had little or no entry defects.

We also examined the ATG mutant virus stability by testing its titer over an extended storage period (Fig. 2D). Viral titer was determined using serial dilutions of worm lysate to test their ability to turn on the GFP in *F26F2.1p*::*GFP* worms. Our data showed that the stability of the mutant and wild-type viruses was comparable up to 10 days (Fig. 2D). Therefore, the observed viral load difference in the media was not caused by difference in viral stability. It is worth noting that all our other experiments used fresh worm lysates, and were completed within five days.

To confirm the viral exit defect in the ATG mutant, we developed a single worm infection assay (Fig. 2E). In this assay, a single infected adult worm was placed on a clean plate with naïve young L1 larvae for a certain time before being removed. When the young L1 worms grew to day-3 adults, they were scored for the Orsay infection symptom of transparent intestine as previously described (12). If a plate of naïve worms had a high infection rate with >50% of worms showing the transparent intestine symptom, we counted this plate as infected. In this assay, infection of naïve worms depended on the amount of virus shed from the single infected worm during the given time window.

The single worm infection assay confirmed that the ATG mutant virus had an exit defect. For wild-type Orsay virus, the amount of virus shed in half an hour from an infected worm was sufficient to infect a plate of worms 67% of the time (Fig. 2F). In contrast, virus shed from a worm infected with the ATG-mutant virus was only sufficient to infect a plate 13% of the time (Fig. 2F). Allowing the worms infected with ATG-mutant viruses to shed virus for a longer time increased the efficacy of infection (Fig. 2F). Sequencing data confirmed that the ATG mutation in the virus was not reverted in

any of the samples, suggesting that the mutant virus could still egress the host although at a lower rate.

δ is located near the apical membrane of host intestine cells

To further investigate δ function, we made transgenic worms expressing GFP-tagged δ under a heat-shock promoter. Upon heat-shock induced synthesis of δ, we observed that δ was predominantly located near the apical membrane in the intestine cells (Fig. 3A). Similarly we investigated CP-δ. From our protein biochemical data (12), it is expected that the proper folding of CP-δ requires the co-expression of CP and CP-δ. Consistent with this, we found that CP-δ formed many aggregates in the absence of CP (Fig. 3B). However, a small soluble portion of CP-δ was located near the apical membrane of the intestine cells, confirming the specificity of δ subcellular localization. In contrast, CP displayed a more ubiquitous cellular localization: near both the apical and the basolateral membrane, in the cytosol, and in the nucleus (Fig. 3C). Therefore, the apical localization is likely specific to δ.

Similar to human epithelial cells, the *C. elegans* intestine cells are polarized cells, with the apical membrane facing the intestinal lumen. The apical membrane is the most likely site where Orsay exits the host cells to be spread to other worms. The apical localization of δ is thus highly consistent with its function in viral exit.

Next we investigated which domain is essential for the apical localization of δ. The N-terminal δ fragment (aa1-66) displayed the apical localization similar to that of the full-length δ (Fig. 3D). In contrast, the C-terminal δ fragment (aa67-346) was diffusively located in the cell (Fig. 3E), suggesting that the N-terminal 66 amino acids are necessary and sufficient to determine the δ apical localization.

δ co-localizes with the host actin ACT-5

Like human epithelial cells, the *C. elegans* intestine cells have microvilli and terminal web on the apical subcellular localization (8) (Fig. 3F). One well-known marker for the apical subcellular localization in *C. elegans* intestine cells is the actin ACT-5. ACT-5 is a unique actin isoform that is exclusively expressed in microvillus-containing cells, and is located in both microvilli and terminal web in the intestine cells (17). To pinpoint the localization of δ, we generated a worm strain that expresses both δ::GFP and mCherry::ACT-5. δ was found to co-localize with ACT-5 (Fig. 3F).

Orsay infection rearranges host actin networks

It was observed that the microsporidia *N. parisii* could rearrange ACT-5 to mediate its non-lytic release from *C. elegans* intestine cells (13). To understand the role of ACT-5 in Orsay infection, we asked whether Orsay infection could cause ACT-5 re-arrangement. To test this, we obtained two marker strains mCherry::ACT-5 and YFP::ACT-5 (18, 19). In both marker strains, ACT-5 fluorescence was observed near the apical membrane of intestine (18, 19). We put these worms on *rde-1* RNAi bacteria to make them sensitive to Orsay infection, and observed ACT-5 localization after viral infection.

Abnormal ACT-5 localization was observed in YFP::ACT-5 animals at 50 hours post Orsay infection, as ACT-5 florescence became weakened at the apical membrane (Fig. 4A). Image quantification revealed that 63% of infected animals had weakened florescence, a significant increase ($p < 0.0001$, Fisher's exact test) from the 7% among uninfected animals (Fig. 4B). When worms were infected with the ATG mutant virus, only 23% of the animals had weakened florescence (Fig. 4B).

To detect whether this weakened florescence was caused by decreased protein amount, we examined the amount of YFP::ACT-5 protein by Western blot. The amount of YFP::ACT-5 remained largely the same after Orsay infection (Fig. 4C), suggesting that the weakened YFP::ACT-5 florescence in infected worms was likely caused by protein relocalization.

Observation at a higher magnification revealed that the actin relocalization appeared to follow the infection time course. ACT-5 relocalization was observed at 24 hours post Orsay infection in anterior intestine cells as abnormal branches formed towards the basolateral side (Fig. 4D, 4E). At 50 hours after Orsay infection, ACT-5 branches were observed in intestine cells more posterior in the worms (Fig. 4F, 4G).

ACT-5 branches were difficult to be quantified in the YFP::ACT-5 line because florescence became weakened at 50 hours post infection. The mCherry::ACT-5 florescence was brighter than the YFP::ACT-5 line, possibly due to a different reporter or a different transgene copy number. The brighter mCherry::ACT-5 line enabled us to better quantify the branching phenotype. At 50 hours after Orsay infection, mCherry::ACT-5 showed several abnormalities, including branches (Fig. 4H), gaps where fluorescence disappeared in one intestine cell (Fig. 4I), and visibly weakened fluorescence. 26% of infected mCherry::ACT-5 animals showed such abnormal ACT-5 localizations, significantly ($p < 0.001$, Fisher's exact test) higher than the 4% observed among uninfected animals (Fig. 4J). Together, these data suggested that Orsay infection induces ACT-5 rearrangement.

δ genetically interacts with the host actin

It was observed that, in comparison with worms infected by the wild-type virus, a significantly reduced number of animals infected by the ATG mutant virus had weakened YFP::ACT-5 fluorescence (23% vs. 63%, $p < 0.0001$, Fisher's exact test, Fig. 4B), suggesting that δ is required to rearrange host actin.

To study δ functional interaction with host actin in intestine cells, we performed *act-5* RNAi by feeding and studied its impact on Orsay infection. As *act-5* RNAi is larval lethal, we diluted the *act-5* RNAi bacteria with control bacteria at a 1:25 ratio. Under these conditions, the *act-5(RNAi)* worms can grow to adults with morphologically normal intestine cells. We infected these worms with wild-type and ATG mutant viruses, and performed single worm infection assay to examine the amount of viruses shed from these animals in 24 hours. Upon infection of the wild-type Orsay virus, *act-5(RNAi)* showed no significant impact on viral egress (Fig. 5A, $p = 0.15$, Student's t-test). However, upon infection of the ATG mutant virus, *act-5(RNAi)* significantly reduced the viral egress efficiency (Fig. 5A, $p = 0.02$, Student's t-test). The combination of *act-5(RNAi)* and δ ATG mutation resulted 16.7% infection rate in this assay, significantly lower than the 43.8% expected from a quantitative epistasis model (20) assuming no genetic interactions between *act-5(RNAi)* and δ ATG mutation (Fig. 5A, $p = 0.04$, Student's t-test). The synergistic effects of *act-5(RNAi)* and δ ATG mutation suggested that δ interacts with ACT-5 functionally to promote efficient viral exit.

Free δ expressed in host cells has biological functions

Free δ was not detected in Western blots (10). One hypothesis is that free δ is produced at a level too low to be detected by the current δ antibody. An alternative

247 hypothesis is that free δ is not produced, and that the viral exit phenotype in the δ ATG
248 mutant virus was caused by defective CP-δ due to the M→L mutation. We have not
249 generated a sensitive antibody to detect free δ, thus we could not rule out the possibility
250 of the second hypothesis. However, several lines of evidence suggested that the second
251 hypothesis is less likely. First, amino acid residues M and L both have hydrophobic side
252 chains that are similar in size, and therefore the mutation is unlikely to disrupt CP-δ
253 folding. Second, mutant Orsay virus with CP-δ fibers containing the point mutation
254 exhibits stability and infection kinetics similar to those of the WT virus (Fig. 2C and 2D).
255 Third, the start codon ATG in the δ ORF is conserved in all three nematode-infecting
256 viruses, Orsay, Santeuil (7) and Le Blanc (9), suggesting a functional requirement for the
257 start codon to express free δ. Lastly, the apical localization of free δ in *C. elegans*
258 intestine cells (Fig. 3) suggested that this protein has specific biological functions.
259 To determine whether free δ can modulate host cell functions on its own, we
260 further examined our transgenic *C. elegans* that ectopically expressed GFP-tagged free δ.
261 In these animals, δ::GFP was expressed under a heat-shock promoter. A few transgenic
262 worms displayed a distal-tip cell (DTC) migration defect when heat-shocked at the L3
263 larval stage during DTC migration (Fig. 5B). While Orsay infects only intestine cells, the
264 heat-shock promoter can drive expression in multiple cell types including the DTC. The
265 DTC migration phenotype suggested that overexpression of free δ caused cytoskeleton
266 rearrangement in the DTC, consistent with our model that δ interacts with actin.
267 If lack of free δ caused the viral exit defect of the δ ATG mutant virus, then
268 providing free δ would rescue such defect. To test this, we exposed both wild-type and
269 transgenic δ::GFP worms to the δ ATG mutant virus. The worms were fed with *rde-1*

RNAi bacteria to make them sensitive to viral infection, and heat shocked to induce the transgene expression. When these worms were tested in the single worm infection assay, the virus shed in 30 minutes from a wild-type worm was unable to infect any plate due to the exit defect of the δ ATG mutant virus (Fig 5C). In contrast, transgenic worms that expressed free δ were able to shed enough virus to infect a plate of naïve worms 23% of the time (Fig. 5C). These data demonstrated that the GFP-tagged free δ is functional and thus its apical localization is of biological relevance. More importantly, the fact that free δ can rescue the viral exit defect of the δ ATG mutant virus suggested that the function of free δ is responsible for the viral exit defect.

Discussion

We showed that the Orsay uses a non-lytic pathway for viral release. The δ ATG mutant virus with a point mutation eliminating the start codon of δ had viral exit defects, demonstrating that δ function is required for efficient viral exit. The ATG mutant virus can still exit host cells although at a lesser efficiency (Fig. 2D). It is possible that there may be leaky protein translation through the CTG initiation codon. An annotation of ten different *E. coli* strains found that 82.5% of the start codons were ATG, 12.3% were GTG and 5% were TTG, with CTG, ATT and ATC used at lower frequencies (21). While no such studies in *C. elegans* have been reported, genetic studies showed that mutation of a single gene *iftb-1* in *C. elegans* allowed a GFP reporter with a GTG start codon to be highly expressed (22), suggesting that a non-ATG initiation is possible in *C. elegans*. It is also possible that there are alternative exit mechanisms that are independent of free δ.

While we found that free δ likely mediates viral exit in this study, we previously reported that δ functions in the fusion protein CP-δ to mediate viral entry, possibly by

293 binding to receptors (12). Therefore, δ appears to have at least two distinct functions in
294 the life cycle of the Orsay virus: viral entry mediated by CP-δ and viral exit mediated by
295 free δ (Fig. 6). While it is unclear whether CP-δ is also involved in viral exit, the ATG
296 mutant virus caused infection symptoms similar to wild-type viruses (Fig. 2), suggesting
297 that free δ is not required for viral entry or replication, but functions in viral exit only.
298 The two distinct functions, viral entry and viral exit, of δ may be carried out by different
299 domains. In CP-δ, δ forms fibers protruding from the viral particle, with its N-terminus
300 fused with CP and its C-terminus forming a globular head at the distal end (12). This
301 structure suggested that the δ C-terminus is likely to mediate viral entry, possibly by host
302 attachment. Indeed, we have shown that δ N-terminus is unlikely to be involved in host
303 attachment, because addition of this protein to the culture media had no impact on viral
304 infection (12). However, expression of the δ N-terminus, but not the C-terminus, is
305 sufficient to carry out the apical localization (Figs. 3D, 3E), suggesting that the N-
306 terminus is involved in viral exit. Overall, these results suggested a model of the δ N-
307 terminus functioning in viral exit and the C-terminus in viral entry.
308 Several results suggested that δ functionally interacts with host ACT-5 to mediate
309 viral exit: 1) δ co-localizes with ACT-5; 2) δ ATG mutant virus failed to rearrange ACT-
310 5 upon infection; 3) Reducing ACT-5 by RNAi exacerbated the viral exit defects of δ
311 ATG mutants. Actin cytoskeleton has been found to play various important roles during
312 the replication life cycle of many viruses (23). Interestingly, instead of being a physical
313 barrier preventing viral exit, ACT-5, a major component of the terminal web, appeared to
314 be promoting Orsay exit (Fig. 5A). It should be noted that our assay exclusively tested
315 viral exit, therefore it is possible that ACT-5 may still function as a barrier to block other

infection steps such as viral entry.

Actin-facilitated viral exit is not unique to Orsay. A similar phenomenon has been observed in rotavirus where actin treadmilling promotes apical viral exit (24), suggesting that the actin-based exit may be utilized by multiple non-enveloped viruses. In another example, the enveloped vaccinia virus induces actin polymerization to facilitate its egress (25). The non-lytic, actin-based exit of Orsay is also similar to that of the microsporidian parasite *N. parisii* (13), despite the large difference in size between the two organisms and the lack of δ-like protein in *N. parisii*. Notably, both Orsay and *N. parisii* are natural intracellular pathogens of *C. elegans* intestinal cells. More studies are needed to reveal the details of such actin functions, for example, how actin facilitates Orsay transportation or membrane remodeling. Future identification of host proteins that physically interacts with Orsay δ will provide further insight into the molecular mechanism of how δ facilitates the non-lytic exit of Orsay.

Materials and Methods

Strains

C. elegans was maintained on standard nematode growth media (NGM) seeded with *E. coli* OP50 as described (26). The wild-type N2 was obtained from the Caenorhabditis Genetics Center (CGC). The transgenic strain used to generate wild-type recombinant virus, *Ex[hsp16-41p::Orsay RNA1+hsp16-41p::Orsay RNA2+pRF4]*, was kindly provided by Dr. David Wang (15). JM125 *caIs[ges-1p::YFP::ACT-5]*III was kindly provided by Dr. James McGhee (17). ERT104 *jyIs17[vha-6p::mCherry::ACT-5+ttx-3p::RFP]* IV and ERT71 *jyIs14[F26F2.1p*::*GFP; myo-2*::*mCherry]* were kindly provided by Dr. Emily Troemel (16, 19).

While N2 is resistant to Orsay infection, inactivation of *rde-1* or *drh-1* genes on N2 background can sensitize the worms to Orsay infection (7, 27). Therefore, all our experiments were conducted on *rde-1(RNAi)*, *rde-1(ne219)*, or *drh-1(ok3495)* background. In addition, the default naïve worms also had the mutation of *glp-4(bn2ts)*. *glp-4(bn2ts)* are sterile at 20°C (28), which allowed us to easily score day-3 adults without interference from progeny.

SS104 *glp-4(bn2ts)* I (28) was kindly provided by Dr. Natasha Kirienko. RB2519 *drh-1(ok3495)* IV was obtained from the CGC, outcrossed six times, and crossed to SS104 to generate *glp-4(bn2ts) I; drh-1(ok3495) IV*. *drh-1* deletion was confirmed by PCR.

Molecular cloning

Plasmids pHIP_RNA1 (*hsp16-41p::Orsay RNA1*) and pHIP_RNA2 (*hsp16-41p::Orsay RNA2*) were kindly provided by Dr. David Wang (15). These plasmids were used as templates to obtain cDNA for each Orsay protein. Amplified viral genes were inserted into the vector pPD118.26 (ligation number L3787, Fire Lab *C. elegans* Vector Kit, Addgene) between *Not* I and *Kpn* I. All constructs were confirmed by sequencing. cDNA for the ATG mutant virus was cloned through mutation PCR using primers to introduce a site mutation to the plasmid pHIP_RNA2.

A truncated Orsay CP (Capsid 42-391) was used in the reporter constructs to remove an NLS-like sequence 10-RKGKPVKQPSS-20 as predicted by the program NLStradamus (29). Orsay CP structure indicated that the first 41 residues of CP are located inside the virion and structurally disordered (30). We have previously shown that

the truncated CP and the full-length CP had almost identical structure and assembly (30). Therefore, the truncated version is likely to reflect CP localization.

Construction of transgenic animals

Micro-injection on N2 young adults were conducted following standard procedures (31). The GFP reporter lines were generated by injecting a mixture of 2-5 ng/μL reporter construct, 5 ng/μL injection marker *myo-2p::DsRed*, and the filler DNA pBlueScript to a total DNA concentration of 200 ng/μL. The recombinant virus lines were generated by injecting a mixture containing 50 ng/μL mutant pHIP_RNA2, 50 ng/μL pHIP_RNA1, and 100 ng/μL pRF4. Transgenic animals were cultured at 15°C to minimize activation of the heat-shock promoter. All transgenes were confirmed by worm PCR and sequencing. ATG mutant virus has also been confirmed by sequencing of RT-PCR product from infected worms. Two independent ATG mutant lines were tested for viral exit defects. Multiple independent lines were tested to confirm the δ localization patterns.

Generation of recombinant virus

A previously published procedure (15) was followed to generate recombinant viruses. 30 roller L4 animals (5 worms/well) were placed on a 6-well RNAi plate that contained NGM, 1mM Isopropyl β-D-1-thiogalactopyranoside (IPTG), and 50 ng/μL Carbenicillin and that was seeded with *rde-1* RNAi bacteria. The worms were cultured for 5 days at 20°C, then heat-shocked at 33°C for 2 hours and maintained at 25°C for 2 days. Worms were fed with IPTG induced *rde*-1 RNAi bacteria throughout the procedure to prevent starvation. The worms were then washed off the plates using the S Basal buffer (26). A mixture of an equal volume of worms and buffer was sonicated on ice. Crude

lysate was centrifuged at 10,000g for 15 min at 4°C. The supernatant was passed through a 0.22 μm filter and kept at 4°C till usage.

Viral infection

Unless otherwise specified, synchronized L1s were exposed to the virus and cultured at 20°C for five days till they were day-3 adults when they were scored. For qRT-PCR, ~300 L1s were dropped into 2 ml of S medium (26). 200 μL worm lysate containing recombinant viruses was added to these worms.

Viral RNA quantification

Worms and media were collected and processed separately. Worms were washed four times with 10 ml S Basal. Culture media were centrifuged at 10,000g at 4°C to remove remaining bacteria. The liquid was passed through a 0.22 μm syringe filter, and concentrated with Amicon Ultra 4, 10K (Millipore, USA) to 100 μL. Total RNA from worms or concentrated media were extracted using Trizol (Invitrogen). RNA was digested with DNase (Invitrogen), and reverse transcribed to cDNA using RETROscript (Thermo). qRT-PCR was performed using PerfeCTa SYBR Green SuperMix (Quantabio). Primers GW194/GW195 and AMA-1F/AMA-1R were used to target Orsay RNA1 and the internal reference gene *ama-1*, respectively (7). Viral Cq values were normalized to *ama-1* values. Viral load of ATG mutant virus were then normalized to that of wild-type virus. Three technical replicates were tested in each trial.

Propidium Iodide (PI) staining

PI (Sigma, Cat. # P4170) staining was conducted as described previously (14, 19). Synchronized *glp-4(bn2ts)*; *rde-1(ne219)* L1 worms were dropped onto NGM seeded with OP50 bacteria and cultured at 20°C till they were day-3 adults. The Cry5B-treated

worms were washed off the plates using M9 buffer, transferred to RNAi plates (NGM with 1mM IPTG, 50 ng/μL Carbenicillin) seeded with Cry5B-OP50 bacteria, and cultured at 25°C for 45 minutes. Cry5B-OP50 bacteria were kindly provided by Dr. Raffi Aroian. Worms were then washed with M9 buffer and transferred to 96-well plates that contained 50μL 5mg/ml serotonin (Sigma, Cat. # H9523) in M9 in each well to force feed the worms. The plates were placed on a 20°C shaker for 15 minutes. 2μL 0.5mg/ml PI was then added to each well to reach a final PI concentration of 20μg/ml. The worms were incubated on the 20°C shaker for additional 30 minutes before being washed by M9 and then scored.

Single worm infection assay

Synchronized L1 worms were infected with viruses and cultured at 20°C till day-3 adults. For Fig. 5C, L1 worms were exposed to the virus, cultured at 20°C for 24 hours, heat shocked at 33°C for 2 hours, and cultured at 25°C till they were day-3 adults. Infected day-3 adults with the transparent intestine phenotype were picked to a test tube containing 10 ml S Basal. Worms were washed twice with S Basal, and dropped to an unseeded NGM plate. Each animal was then picked to a new NGM plate that contained ~100 L1 *glp-4(bn2)*;*rde-1(ne219)* worms, and removed after a certain time. For Fig. 5A, these new plates were RNAi plates seeded with *act-5* RNAi bacteria (1:25 diluted with control bacteria) to maintain *act-5* RNAi effects on the original infective worm. As *rde-1(ne219)* is resistant to RNAi, *act-5* RNAi had no impact on these naïve worms. The L1 naïve worms were cultured at 20°C till they were day-3 adults. A plate with >50% worms showing the transparent intestine phenotype was scored as infected. Biological replicates

were obtained using naïve L1s collected from different batches of parental animals, and recombinant viruses generated from different batches of transgenic worms.

Determination of viral infection kinetics

About 90 synchronized L1 larvae of *jyIs14* worms were cultured on a 3cm NGM plate seeded with OP50 at 20°C for 24 hours. A mixture of 10μL water and 10μL crude worm lysate containing recombinant viruses was added to the plate. GFP positive worms were counted and removed every two hours. In this assay and the following titer assay examining viral stability, a control group of uninfected worms was always tested to ensure that no GFP was observed there.

Determination of viral stability

Aliquots of virus-containing worm lysate were tested for relative titer on different dates. To test relative titer, lysate was diluted in water to 5%, 2.5%, 1.25%, 0.63%, 0.31%, 0.16%, 0.08%, and 0.04%. About 90 synchronized L1 larvae of *jyIs14* worms were placed on a 3cm NGM plate and exposed to 20μL of diluted virus. Four worm plates were tested for each viral dilution. The worms were observed after being cultured at 20°C for three days when they were adults. A plate with at least five GFP-positive worms was counted as infected. The most diluted viral concentration that had at least two infected plates was used. Viral titer was divided by day 1 titer to obtain relative titer.

Western blot

JM125 worms were fed with IPTG induced *rde-1* RNAi bacteria and grown in 50ml liquid culture as described (26). For the infected group, 500μL of viral filtration (7) was added at the beginning of the liquid culture. Infected and uninfected worms were cultured at 20°C for 6 days before pelleted and sonicated in lysis buffer containing 50 mM Tris

pH8.0, 300 mM NaCl, 10% glycerol (v/v), 5 mM 2-Mercaptoethanol (2-ME), 1 mM NaN_3 and 1 mM phenylmethylsulfonyl fluoride (PMSF). Total cell lysates were resolved on 15% SDS-PAGE gel and transferred to polyvinylidene difluoride (PVDF) membrane. After blocking with 5% milk in Tris-buffered saline (TBS, pH 7.4) containing 0.1% Tween-20 (TBST), Membranes were probed with antibodies for YFP (G1544, Sigma) and tubulin (loading control) (T9026, Sigma) overnight at 4°C. Membranes were then washed three times with TBST and incubated with HRP conjugated secondary antibodies for one hour at 4°C. After washed three times with TBST, immune-reactive bands were detected using SIGMAFAST™ BCIP®/NBT alkaline phosphatase substrate (Sigma). Intensities of various analyte proteins and their respective loading controls from the same blot were measured using the program Fiji (32). The amount of ACT-5 in each sample was quantitated by dividing the intensity of the ACT-5 band by that of the loading control.

Microscopy

Epifluorescent images were taken using a Zeiss AxioImager M2m microscope equipped with a Zeiss AxioCam MRm camera. The software AxioVision 4.8 was used for camera control. To quantify YFP::ACT-5 expression level, images were taken using the same exposure time. Pixel brightness and the number of bright pixels were measured using the software PhenoCapture 3.3 (PhenoCapture.com). For the δ localization experiment, to induce the heat-shock promoter in these GFP-reporter lines, transgenic worms were placed in 33°C water bath for 2 hours, and then recovered at 20°C for 90 minutes before being observed. *jyIs14* GFP was observed under a Zeiss SteReo Discovery V20 stereoscope.

475 # Acknowledgments

476 We thank Drs. James McGhee, Emily Troemel, David Wang, Raffi Aroian for reagents,
477 Boanerges Aleman-Meza and Matthew Ykema for comments on the manuscript, and
478 Joaquina Nunez for technical support. We thank the Caenorhabditis Genetics Center
479 (CGC) which was funded by NIH Office of Research Infrastructure Programs (grant P40
480 OD010440) for providing strains. This work was supported by the Robert A. Welch
481 Foundation (C-1565 to YJT), the Hamill Foundation (the Hamill Award at Rice
482 University to YJT and WZ), the National Institutes of Health (R01-AI122356 to YJT and
483 WZ). The funders had no role in study design, data collection and analysis, decision to
484 publish, or preparation of the manuscript.
485

References

1. Smith GA, Enquist LW. 2002. Break ins and break outs: viral interactions with the cytoskeleton of Mammalian cells. Annu Rev Cell Dev Biol 18:135–161.

2. Blank CA, Anderson DA, Beard M, Lemon SM. 2000. Infection of polarized cultures of human intestinal epithelial cells with hepatitis A virus: vectorial release of progeny virions through apical cellular membranes. J Virol 74:6476–6484.

3. Tucker SP, Thornton CL, Wimmer E, Compans RW. 1993. Vectorial release of poliovirus from polarized human intestinal epithelial cells. J Virol 67:4274–4282.

4. Clayson ET, Brando LV, Compans RW. 1989. Release of simian virus 40 virions from epithelial cells is polarized and occurs without cell lysis. J Virol 63:2278–2288.

5. Jourdan N, Maurice M, Delautier D, Quero AM, Servin AL, Trugnan G. 1997. Rotavirus is released from the apical surface of cultured human intestinal cells through nonconventional vesicular transport that bypasses the Golgi apparatus. J Virol 71:8268–8278.

6. Marsh EK, May RC. 2012. Caenorhabditis elegans, a Model Organism for Investigating Immunity. Appl Environ Microbiol 78:2075–2081.

7. Félix M-A, Ashe A, Piffaretti J, Wu G, Nuez I, Bélicard T, Jiang Y, Zhao G, Franz CJ, Goldstein LD, Sanroman M, Miska EA, Wang D. 2011. Natural and experimental infection of Caenorhabditis nematodes by novel viruses related to nodaviruses. PLoS Biol 9:e1000586.

8. McGhee J. 2007. The C. elegans intestine. WormBook.

9. Franz CJ, Zhao G, Félix M-A, Wang D. 2012. Complete genome sequence of Le Blanc virus, a third Caenorhabditis nematode-infecting virus. J Virol 86:11940.

10. Jiang H, Franz CJ, Wu G, Renshaw H, Zhao G, Firth AE, Wang D. 2014. Orsay virus utilizes ribosomal frameshifting to express a novel protein that is incorporated into virions. Virology 450–451:213–221.

11. Guo X, Lu R. 2013. Characterization of virus-encoded RNA interference suppressors in Caenorhabditis elegans. J Virol 87:5414–5423.

12. Fan Y, Guo YR, Yuan W, Zhou Y, Holt MV, Wang T, Demeler B, Young NL, Zhong W, Tao YJ. 2017. Structure of a pentameric virion-associated fiber with a potential role in Orsay virus entry to host cells. PLoS Pathog 13:e1006231.

13. Estes KA, Szumowski SC, Troemel ER. 2011. Non-lytic, actin-based exit of intracellular parasites from C. elegans intestinal cells. PLoS Pathog 7:e1002227.

14. Los FCO, Kao C-Y, Smitham J, McDonald KL, Ha C, Peixoto CA, Aroian RV. 2011. RAB-5- and RAB-11-dependent vesicle-trafficking pathways are required for plasma membrane repair after attack by bacterial pore-forming toxin. Cell Host Microbe 9:147–157.

15. Jiang H, Franz CJ, Wang D. 2014. Engineering Recombinant Orsay Virus Directly in the Metazoan Host C. elegans. J Virol. 88:11774-11781.

16. Bakowski MA, Desjardins CA, Smelkinson MG, Dunbar TA, Lopez-Moyado IF, Rifkin SA, Cuomo CA, Troemel ER. 2014. Ubiquitin-Mediated Response to Microsporidia and Virus Infection in C. elegans. PLoS Pathog 10:e1004200.

17. MacQueen AJ, Baggett JJ, Perumov N, Bauer RA, Januszewski T, Schriefer L, Waddle JA. 2005. ACT-5 Is an Essential Caenorhabditis elegans Actin Required for Intestinal Microvilli Formation. Mol Biol Cell 16:3247–3259.

18. Bossinger O, Fukushige T, Claeys M, Borgonie G, McGhee JD. 2004. The apical disposition of the Caenorhabditis elegans intestinal terminal web is maintained by LET-413. Dev Biol 268:448–456.

19. Szumowski SC, Estes KA, Popovich JJ, Botts MR, Sek G, Troemel ER. 2016. Small GTPases promote actin coat formation on microsporidian pathogens traversing the apical membrane of Caenorhabditis elegans intestinal cells. Cell Microbiol 18:30–45.

20. Baryshnikova A, Costanzo M, Myers CL, Andrews B, Boone C. 2013. Genetic interaction networks: toward an understanding of heritability. Annu Rev Genomics Hum Genet 14:111–133.

21. Villegas A, Kropinski AM. 2008. An analysis of initiation codon utilization in the Domain Bacteria - concerns about the quality of bacterial genome annotation. Microbiol Read Engl 154:2559–2661.

22. Zhang Y, Maduzia LL. 2010. Mutations in Caenorhabditis elegans eIF2beta permit translation initiation from non-AUG start codons. Genetics 185:141–152.

547 23. Taylor MP, Koyuncu OO, Enquist LW. 2011. Subversion of the actin cytoskeleton
548 during viral infection. Nat Rev Microbiol 9:427–439.

549 24. Gardet A, Breton M, Trugnan G, Chwetzoff S. 2007. Role for Actin in the Polarized
550 Release of Rotavirus. J Virol 81:4892–4894.

551 25. Snetkov X, Weisswange I, Pfanzelter J, Humphries AC, Way M. 2016. NPF motifs
552 in the vaccinia virus protein A36 recruit intersectin-1 to promote Cdc42:N-WASP-
553 mediated viral release from infected cells. Nat Microbiol 1:16141.

554 26. Stiernagle T. 2006. Maintenance of C. elegans. WormBook.

555 27. Ashe A, Bélicard T, Pen JL, Sarkies P, Frézal L, Lehrbach NJ, Félix M-A, Miska
556 EA. 2013. A deletion polymorphism in the Caenorhabditis elegans RIG-I homolog
557 disables viral RNA dicing and antiviral immunity. eLife 2:e00994.

558 28. Beanan MJ, Strome S. 1992. Characterization of a germ-line proliferation mutation
559 in C. elegans. Dev Camb Engl 116:755–766.

560 29. Nguyen Ba AN, Pogoutse A, Provart N, Moses AM. 2009. NLStradamus: a simple
561 Hidden Markov Model for nuclear localization signal prediction. BMC
562 Bioinformatics 10:202.

563 30. Guo YR, Hryc CF, Jakana J, Jiang H, Wang D, Chiu W, Zhong W, Tao YJ. 2014.
564 Crystal structure of a nematode-infecting virus. Proc Natl Acad Sci U S A
565 111:12781–12786.

566 31. Evans T. 2006. Transformation and microinjection. WormBook.

32. Schindelin J, Arganda-Carreras I, Frise E, Kaynig V, Longair M, Pietzsch T, Preibisch S, Rueden C, Saalfeld S, Schmid B, Tinevez J-Y, White DJ, Hartenstein V, Eliceiri K, Tomancak P, Cardona A. 2012. Fiji: an open-source platform for biological-image analysis. Nat Methods 9:676–682.

Figure legend

Fig 1. Orsay has non-lytic exit. Propidium iodide (PI) staining of uninfected (A), Cry5B-treated (B), and Orsay infected (C) animals. Left to right, the images show PI staining, merged PI staining and Normaski image, merged PI staining and autofluorescence in the blue channel. *, intracellular regions that were not stained by PI. Scale bar, 10 μm.

Fig 2. ATG mutant virus has exit defects. (A) Schematic drawing of the strategy for recombinant virus generation. (B) qRT-PCR results showing viral load in infected worms and in culture media. Data were from three biological replicates, each with three technical replicates. Bar and error bars show mean and standard error (SE). ** $p < 0.01$, Student's t-test. (C) Viral infection kinetics based on the *F26F2.1p*::*GFP* expression in infected worms. n≥529 worms for each time point. Data compiled from three independent trials with six plates for each virus genotype in each trial. (D) Viral titer of the worm lysate over storage time. Titer was normalized so that fresh lysate (Day 1) had a relative titer of 1. (E) Schematic drawing of the single worm infection assay. (F) Single worm infection assay results comparing the ATG mutant virus and wild-type. Data were from four independent trials, each with six plates for each time point. Graph displays mean and SE.

Fig 3. Free δ is localized near the apical membrane in intestine cells. (A-E) Normaski and florescence images showing the subcellular localization of GFP tagged δ (A), CP-δ (B), CP (C), N-terminal 1-66 aa of δ (D), and C-terminal 67-346 aa of δ (E). Arrowheads

596 indicate apical and basolateral membrane localization. * indicates nuclear localization.
597 Arrows indicate aggregates. (F) Co-localization of δ and ACT-5. The schematic drawing
598 shows ACT-5 localization in an intestine cell. Scale bar, 10 μm.
599
600 **Fig 4**. **Orsay infection rearranges the ACT-5 actin structure.** (A) YFP::ACT-5
601 localization at the apical membrane is weakened 50 hours after Orsay infection. Scale
602 bar, 100 μm. (B) The percentage of animals with weak YFP::ACT-5 in uninfected
603 worms, worms infected with wild-type virus, and worms infected with the ATG mutant
604 virus. ***. $p < 0.001$, Fisher's exact test. $n \geq 125$ animals for each group. (C) Western
605 blot. Tubulin was used as a loading control. Graph displays mean and standard error of
606 data from two biological replicates, each with five technical replicates. N.S., not
607 significant. (D-I) Orsay infection causes ACT-5 to have branches and gaps. At 24 hours
608 after Orsay infection, YFP::ACT-5 branches appear in anterior cells of infected (E) but
609 not uninfected worms (D). At 50 hours after infection, YFP::ACT-5 branches appear in
610 cells close to the midbody of infected (G) but not uninfected (F) worms. Also at 50 hours
611 after infection, branches (H) and gaps (I) can be observed in mCherry::ACT-5. Scale bar,
612 10 μm. (J) The percentage of animals with abnormal mCherry::ACT-5 in uninfected and
613 infected worms. **. $p < 0.01$, Fisher's exact test. $n \geq 69$ animals for each group. For
614 quantification purpose, if a worm showed multiple phenotypes, it was classified in the
615 category of its most severe phenotype, following the phenotypic severity order of gap >
616 branch > weak (from severe to weak).
617

Fig 5. Free δ has biological functions. (A) δ genetically interacts with *act-5*. Single worm infection assay results showing effects of the δ ATG mutation in virus and *act-5(RNAi)* on hosts. Data are from four independent trials, each with six plates for each genotype. Graph displays mean and SE. N.S., not significant. * $p < 0.05$, Student's t-test. (B) Normaski images showing the distal tip cell (DTC) migration defects in some worms upon heat-shock-induced overexpression of δ::GFP. Scale bar, 10 μm. Schematic line drawings under the images show the DTC migration path. (C) Single worm infection assay results showing effects of expressing δ::GFP in host cells rescued the viral exit defects of the δ ATG mutant virus. Data are from five independent trials, with 6 or 12 plates for each genotype in each trial. Graph displays mean and SE. * $p < 0.05$, Student's t-test.

Fig 6. Proposed model of δ functions. δ may function in both viral entry and exit. In the CP-δ fusion, δ may mediate viral entry possibly by interacting with cell surface receptors. The free δ may interact with ACT-5 to promote polarized viral exit. Proteins are color coded: orange represents the pentameric δ fiber; green highlights the Orsay capsid; red indicates ACT-5.

FIG 1

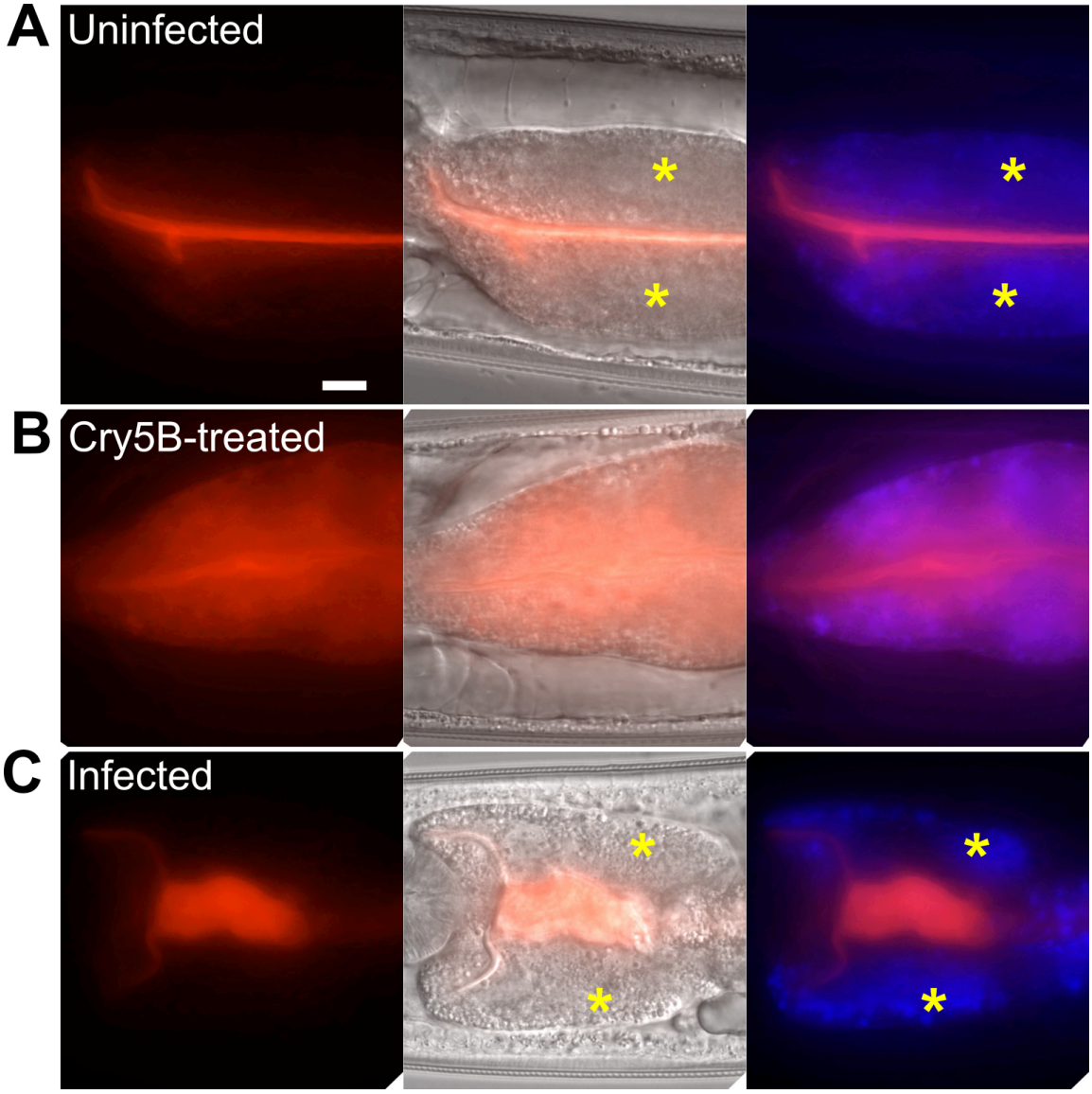

Fig 1. Orsay has non-lytic exit. Propidium iodide (PI) staining of uninfected (A), Cry5B-treated (B), and Orsay infected (C) animals. Left to right, the images show PI staining, merged PI staining and Normaski image, merged PI staining and autofluorescence in the blue channel. *, intracellular regions that were not stained by PI. Scale bar, 10 μm.

FIG 2

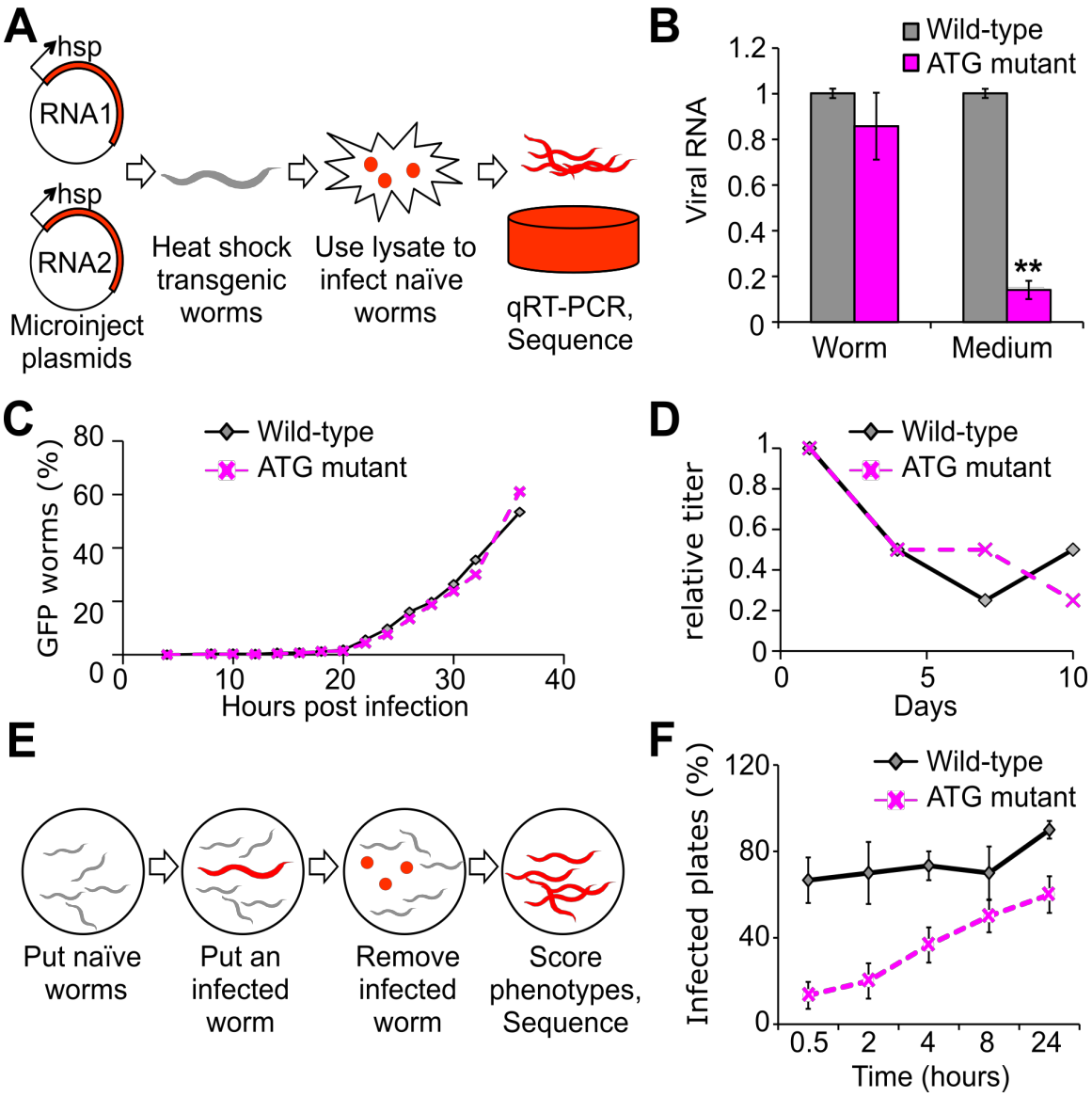

Fig 2. ATG mutant virus has exit defects. (A) Schematic drawing of the strategy for recombinant virus generation. (B) qRT-PCR results showing viral load in infected worms and in culture media. Data were from three biological replicates, each with three technical replicates. Bar and error bars show mean and standard error (SE). ** $p < 0.01$, Student's t-test. (C) Viral infection kinetics based on the *F26F2.1p*::*GFP* expression in infected worms. n≥529 worms for each time point. Data compiled from three independent trials with six plates for each virus genotype in each trial. (D) Viral titer of the worm lysate over storage time. Titer was normalized so that fresh lysate (Day 1) had a relative titer of 1. (E) Schematic drawing of the single worm infection assay. (F) Single worm infection assay results comparing the ATG mutant virus and wild-type. Data were from four independent trials, each with six plates for each time point. Graph displays mean and SE.

FIG 3

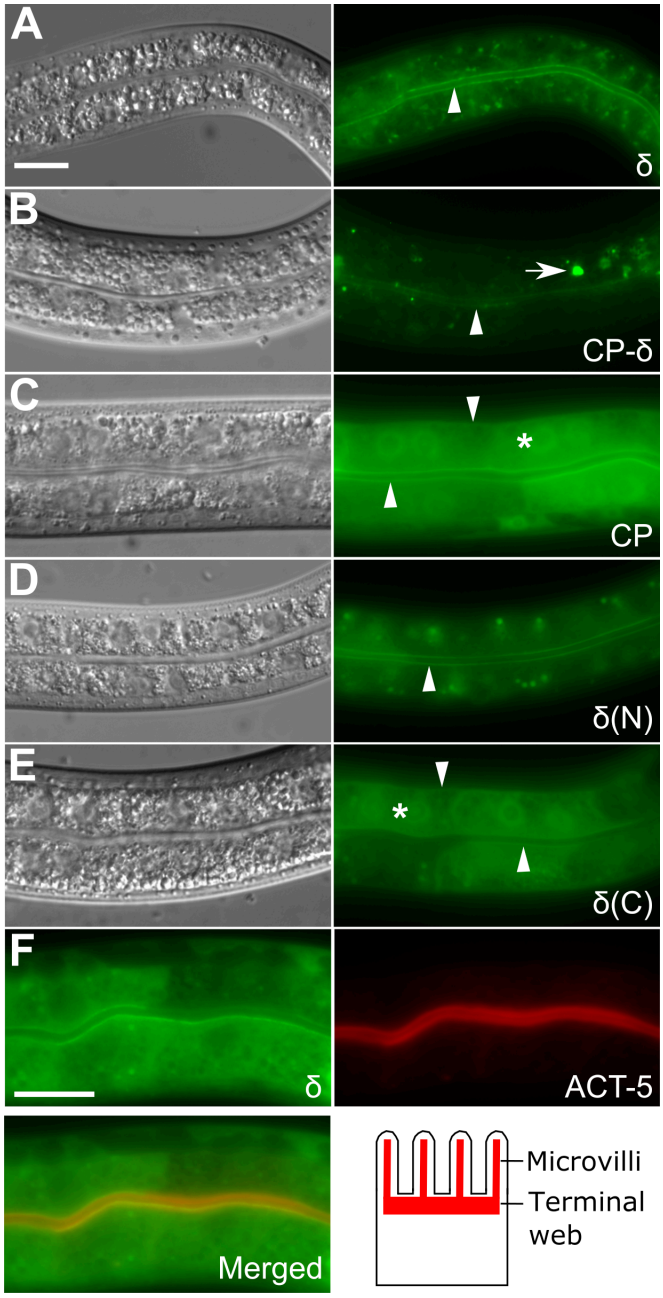

Fig 3. Free δ is localized near the apical membrane in intestine cells. (A-E) Normaski and florescence images showing the subcellular localization of GFP tagged δ (A), CP-δ (B), CP (C), N-terminal 1-66 aa of δ (D), and C-terminal 67-346 aa of δ (E). Arrowheads indicate apical and basolateral membrane localization. * indicates nuclear localization. Arrows indicate aggregates. (F) Co-localization of δ and ACT-5. The schematic drawing shows ACT-5 localization in an intestine cell. Scale bar, 10 μm.

FIG 4

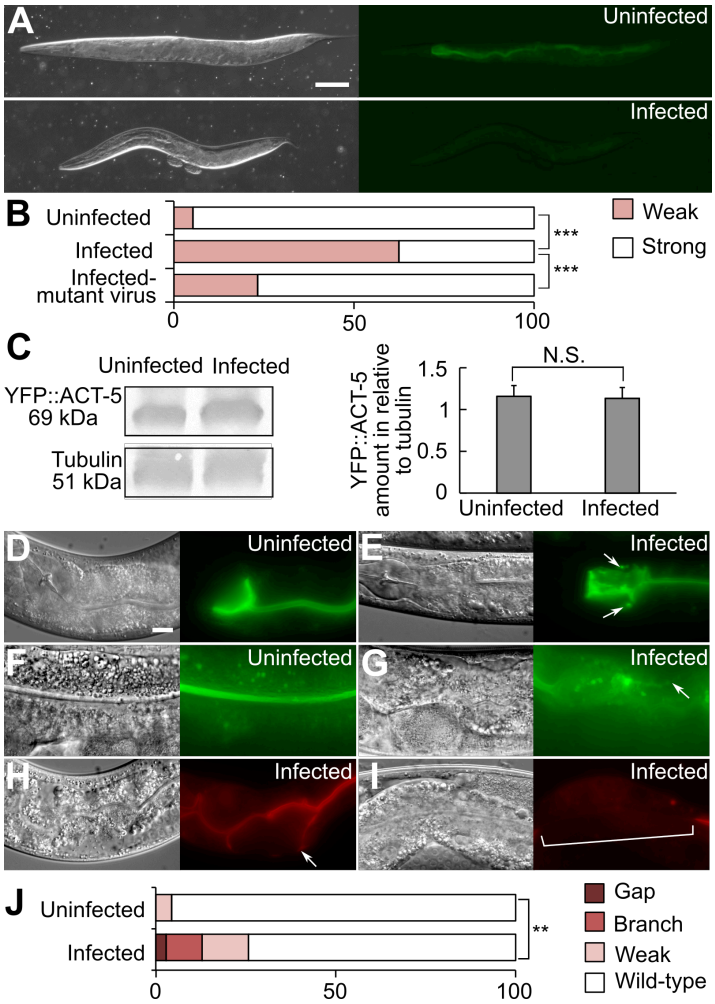

Fig 4. **Orsay infection rearranges the ACT-5 actin structure.** (A) YFP::ACT-5 localization at the apical membrane is weakened 50 hours after Orsay infection. Scale bar, 100 μm. (B) The percentage of animals with weak YFP::ACT-5 in uninfected worms, worms infected with wild-type virus, and worms infected with the ATG mutant virus. ***. $p < 0.001$, Fisher's exact test. $n \geq 125$ animals for each group. (C) Western blot. Tubulin was used as a loading control. Graph displays mean and standard error of data from two biological replicates, each with five technical replicates. N.S., not significant. (D-I) Orsay infection causes ACT-5 to have branches and gaps. At 24 hours after Orsay infection, YFP::ACT-5 branches appear in anterior cells of infected (E) but not uninfected worms (D). At 50 hours after infection, YFP::ACT-5 branches appear in cells close to the midbody of infected (G) but not uninfected (F) worms. Also at 50 hours after infection, branches (H) and gaps (I) can be observed in mCherry::ACT-5. Scale bar, 10 μm. (J) The percentage of animals with abnormal mCherry::ACT-5 in uninfected and infected worms. **. $p < 0.01$, Fisher's exact test. $n \geq 69$ animals for each group. For quantification purpose, if a worm showed multiple phenotypes, it was classified in the category of its most severe phenotype, following the phenotypic severity order of gap > branch > weak (from severe to weak).

FIG 5

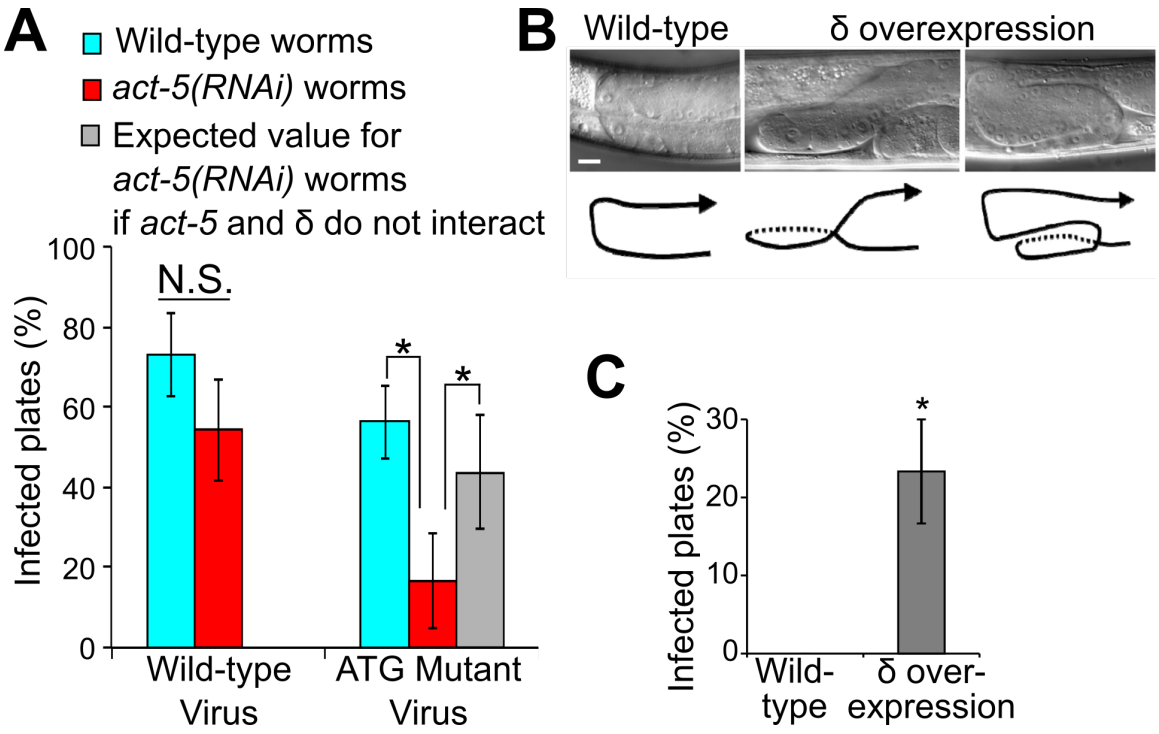

Fig 5. Free δ has biological functions. (A) δ genetically interacts with *act-5*. Single worm infection assay results showing effects of the δ ATG mutation in virus and *act-5(RNAi)* on hosts. Data are from four independent trials, each with six plates for each genotype. Graph displays mean and SE. N.S., not significant. * $p < 0.05$, Student's t-test. (B) Normaski images showing the distal tip cell (DTC) migration defects in some worms upon heat-shock-induced overexpression of δ::GFP. Scale bar, 10 μm. Schematic line drawings under the images show the DTC migration path. (C) Single worm infection assay results showing effects of expressing δ::GFP in host cells rescued the viral exit defects of the δ ATG mutant virus. Data are from five independent trials, with 6 or 12 plates for each genotype in each trial. Graph displays mean and SE. * $p < 0.05$, Student's t-test.

FIG 6

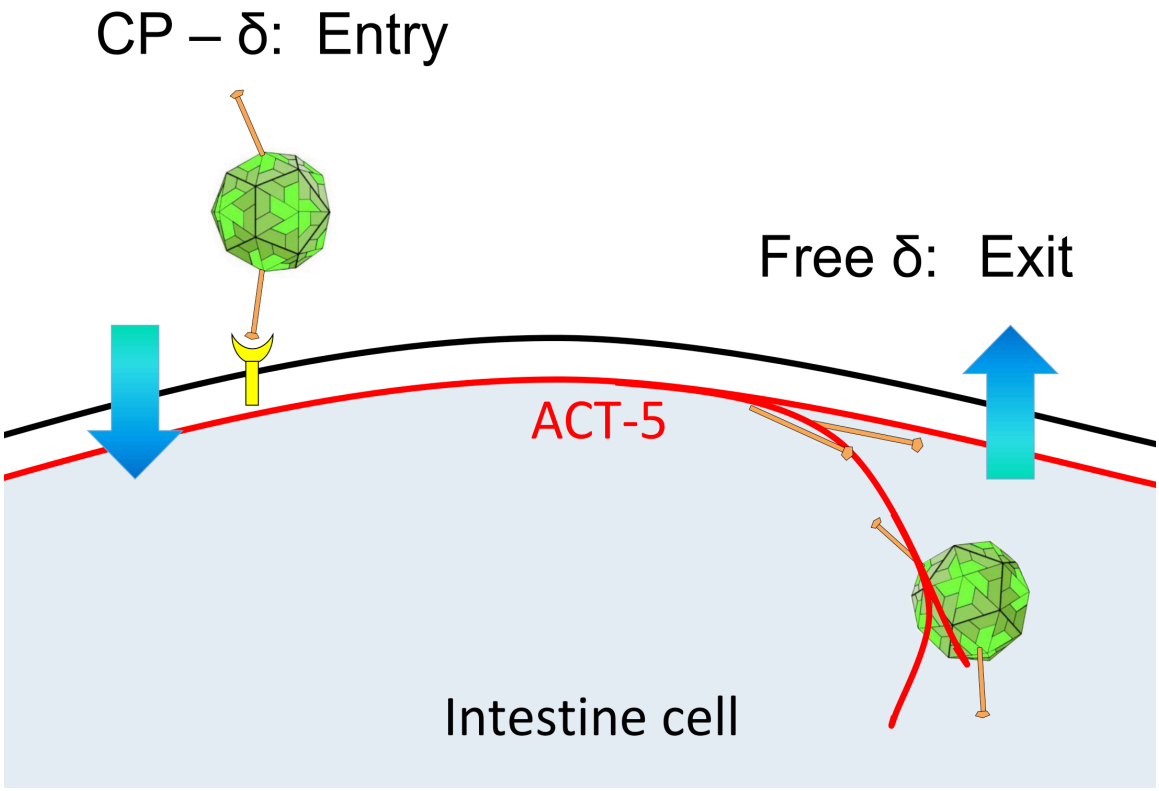

Fig 6. Proposed model of δ functions. δ may function in both viral entry and exit. In the CP-δ fusion, δ may mediate viral entry possibly by interacting with cell surface receptors. The free δ may interact with ACT-5 to promote polarized viral exit. Proteins are color coded: orange represents the pentameric δ fiber; green highlights the Orsay capsid; red indicates ACT-5.

A

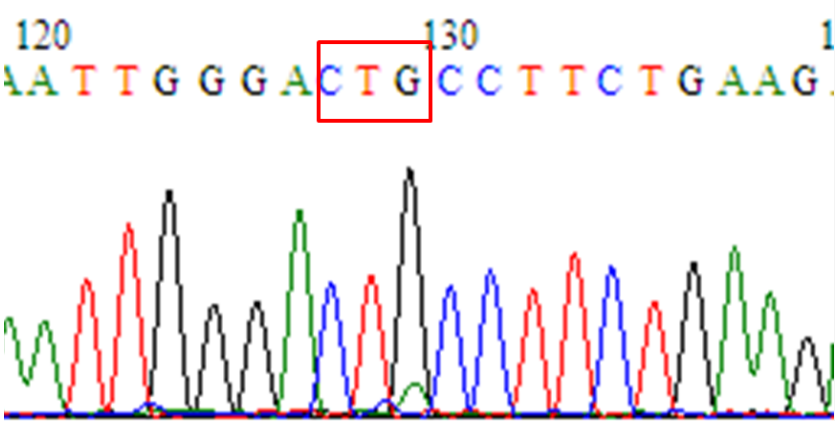

B

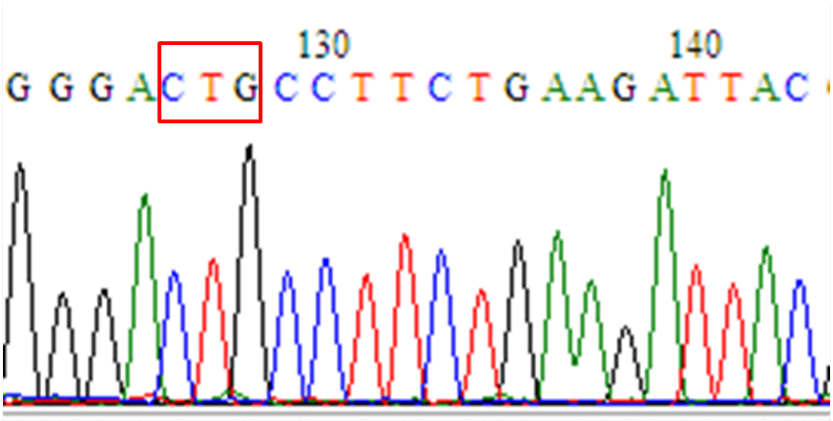

Figure S1. Representative sequencing results from single-worm infection assays using the ATG-CTG mutant virus. Worms were exposed to worm lysates containing recombinant viruses. An infected day-3 adult worm was then placed on a new plate with naïve L1 worms for 30 minutes (A) or 24 hours (B) before being removed. When the L1 worms grew up to day-3 adults, RNA was extracted from them and RT-PCR was performed. The DNA product was sequenced. Red box highlights that the ATG-to-CTG mutation was maintained in the mutant virus.